Sampling Robustness in Gradient Analysis of Urban Material Mixtures

Chaonan Ji, Marianne Jilge, Uta Heiden, Marion Stellmes, and Hannes Feilhauer

Abstract—**Many studies analyzing spaceborne hyperspectral images (HSIs) have so far struggled to deal with a lack of pure pixels due to complex mixtures of urban surface materials. Recently, an alternative concept of gradients in urban surface material composition has been proposed and successfully applied to map cities with spaceborne HSIs without the requirement for a previous determination of pure pixels. The gradient concept treats all pixels as mixed and aims to describe and quantify gradual transitions in the cover fractions of surface materials. This concept presents a promising approach to tackle urban mapping using spaceborne HSIs. However, since gradients are determined in a data-driven way, their transferability within urban areas needs to be investigated. For this purpose, we analyze the robustness of urban surface material gradients and their dependence across six systematic and three simple random sampling schemes. The results show a high similarity between nine sampling schemes in the primary gradient feature space (Pspace) and individual gradient feature spaces (Ispaces). In comparing the Pspace to the Ispaces, the Mantel statistics shows the resemblance of samples' distribution in the Pspace and each Ispace is rather strong with high credibility, as the significance level is P < 0.01. Therefore, it can be concluded that material gradients defined in the test area are independent of the specific sampling scheme. This study paves the way for subsequent analysis of the stability of urban surface material gradients and the interpretation of material gradients in other urban environments.**

Index Terms—**Hyperspectral images, gradient analysis, sampling robustness, urban mapping, transferability**

I. Introduction

The structure and patterns of urban developments have a large effect on urban ecosystem functions [1]. Urban surface conditions strongly influence the climate within cities in the micro scale as well as in the meso and macro scale [2]. To better understand the climatic interactions within the urban ecosystem, urban surface material compositions are of great interest for climate modelers [3]. By providing global coverage of pixel-based spectral signatures, spaceborne HSIs can supply substantial information about ecosystem characteristics [4]. However, the spatial resolution of most operating and future spaceborne HSIs (e.g., EnMAP [5], PRISMA [6], DESIS [7], [8] and HISUI [9]) leads to high spectral mixtures in urban areas [10], [11]. Therefore, urban mapping at this spatial scale is still a challenge due to a lack of spectrally pure pixels to train classifiers [12].

Nevertheless, the mixture within a pixel of urban materials is not arbitrary. In many cases, the actual land use determines the dominant materials that are used for building structures and their surroundings [13], [14]. For example, industrial areas are often characterized by a co-occurrence of concrete, asphalt, and metal roofing; residential areas frequently feature roofing tiles, trees and lawns. Historical city quarters in Germany such as Wilhelminian style quarters commonly contain roofing tiles, cobblestones pavements for streets, trees and copper roofs [15]–[17]. The distribution of these urban neighborhoods thus leads to reoccurring combinations of material compositions that show strongly inter-correlated distribution patterns [10], [18].

The nature of co-occurring surface materials in urban neighborhoods has been the underlying basis for a new technique to analyze urban surface material mixtures. [10] could successfully introduce the gradient concept for urban areas using a test site in Munich, Germany, to relate the distribution patterns of urban surface material compositions to urban neighborhoods. So far, the gradient concept has only been used by vegetation ecologists to characterize floristic gradients for mapping continuous and discrete patterns in plant species assemblages [19]–[22]. Treating the mixture of urban surface materials in analogy to the species assemblages in natural vegetation stands, [10] proofed the existence of urban material gradients. The similarity of the surface material composition collected by 153 samples was explored by a feature reduction method (detrended correspondence analysis, DCA). The resulting gradient scores have been regressed against simulated hyperspectral EnMAP data that have a spatial resolution of 30 m x 30 m pixel size. The resulting gradient maps showed pattern of similar urban surface material mixtures that could be linked to specific urban neighborhoods such high density block developments (Wilhelminian style quarter), industrial areas and detached house developments.

However, due to the data-driven property of the gradient analysis, the applicability of this approach for other urban areas needs to be further analyzed. Important aspects of the analyses are the impact of the developed training data on the

Chaonan Ji is with the Humboldt Universität zu Berlin, Geography Department, Rudower Chaussee 16, 12489 Berlin, and also with the German Aerospace Center (DLR), German Remote Sensing Data Center (DFD), Oberpfaffenhofen, 82234 Wessling, Germany. (e-mail: ji.chaonan@dlr.de)

Jilge Marianne is with the German Aerospace Center (DLR), German Remote Sensing Data Center (DFD), Oberpfaffenhofen, 82234 Wessling, Germany (e-mail: marianne.jilge@dlr.de)

Uta Heiden is with the German Aerospace Center (DLR), Remote Sensing Technology Institute (IMF), Oberpfaffenhofen, 82234 Wessling, Germany (e-mail: uta.heiden@dlr.de)

Marion Stellmes is with the Freie Universität Berlin, Institute of Geographical Sciences, Malteserstr. 74-100, 12249 Berlin, Germany (e-mail: marion.stellmes@fu-berlin.de

Hannes Feilhauer is with the Universität Leipzig, Institute for Geography & Remote Sensing Center for Earth System Research, Talstr. 35, 04103 Leipzig, Germany and with the Freie Universität Berlin, Institute of Geographical Sciences, Malteserstr. 74-100, 12249 Berlin, Germany (e-mail: hannes.feilhauer@uni-leipzig.de)

gradient feature space, the regression model stability and the gradient interpretation.

In this paper, we evaluate the impact of the design of the training data sampling on the resulting gradient feature space. Mainly, we aim to answer the following three questions: (1) Does the slight movement of systematic sampling affect the material gradients? (2) Are material gradients influenced by using random sampling schemes rather than systematic sampling schemes? (3) To better derive surface material compositions for urban areas, what other possible factors could influence the material gradients? Referring to the sampling scheme of the proof-of-concept study [10], we examine five additional systematical sampling schemes with regular offsets and three random sampling schemes and analyze the impact on the gradient feature space.

The paper is organized as follows. Section II provides a background of the study area and the used data sets. Section III describes the methodology of the experiment, whose experimental results follow in Section IV. A comprehensive discussion is presented in Section V. Finally, Section VI concludes this paper.

II. STUDY AREA AND DATA

A. Study Area

The study area (Fig. 1) is located in the city of Munich, Germany, the same test site as in the study of Jilge et al. [10]. It covers 4.12 km^2 from 48.106°N to 48.133°N and from 11.565°E to 11.632°E. The Isar river divides the study area into two parts. The northwestern part is mainly occupied by old buildings from the Wilhelmine era. In the southeast part, a large vegetated cemetery is situated in the center, surrounded by the Munich East Railway Station, industrial areas, and various residential and commercial areas. The large variety of urban surface materials and their specific compositions are typical for large German cities and provide ideal conditions for investigating the robustness of material gradients among different sampling schemes.

B. Data

A detailed surface material map (Fig. 1) was used to sample the material composition as the ground truth in order to define the material gradients. The surface material map was prepared by Helden et al. [17] based on airborne HSI with a spatial resolution of 4 m x 4 m, recorded with the HyMap sensor [23] in a flight campaign in June 2007, and pre-processed by [24]–[26] . The surface material map initially contained 42 material classes. The modified surface material map removed unlabeled pixels, shadow pixels, facade pixels, and materials which were not covered by every sampling scheme. Finally, 27 urban surface material classes were selected analogous to [10]. For more details about the pre-processing of the HSI data and the accuracy of the surface material map, interested readers are referred to [10], [16], [17] and the references therein.

III. METHODOLOGY

A schematic work flow of the proposed approach for sampling robustness analysis of material gradient is shown
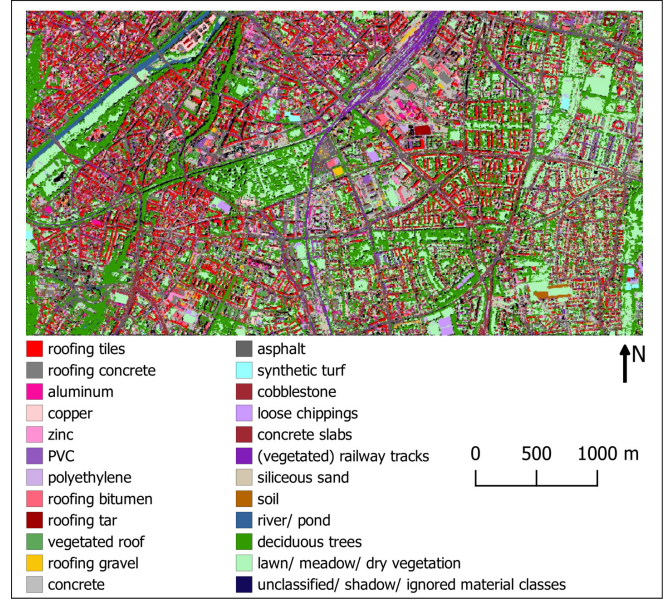

Fig. 1. Detailed urban surface material map of the study area in Munich, Germany, determined from HyMap data. Each color represents an urban surface material.

in Fig. 2. In subsection A, six systematic and three simple random sampling schemes are designed. For each sampling scheme, the surface material compositions of each sample are acquired. Subsection B introduces why and how to define material gradients via principle component analysis (PCA). In subsection C, the gradient feature space generated by one sampling scheme ($o4$) is defined as the primary gradient feature space (Pspace). For the visual comparison of the sample distribution in the feature space, all samples from each sampling scheme are projected into the Pspace. The transformation matrix from the original material composition matrix into the gradient score matrix of samples is referred to as loadings. In subsection D, each sampling scheme generate its individual gradient feature space (Ispace). Loadings from Ispaces are compared with each other, and the multiple linear regressions of material gradients and the corresponding urban surface materials are analyzed for the similarity of Ispaces. In subsection E, the Pspace is further compared with each Ispace by a Mantel test and a Procrustes analysis to check the similarity between the Pspace and Ispaces.

A. Sampling design

The sampling robustness of gradients is defined as the transferability and generalizability of material gradients that are applicable to other sampling schemes. For this purpose, this study attempts to assess the similarity of the material gradients generated from different sampling schemes. To analyze the robustness of material gradients, different distributions of samples across the study area are required, which are determined by systematic and simple random sampling schemes. The systematic sampling scheme is intended to support a transition of surface material compositions between neighboring systematic sampling schemes (e.g., $s1$ and $s2$ in Fig. 2). The simple random sampling schemes do not follow
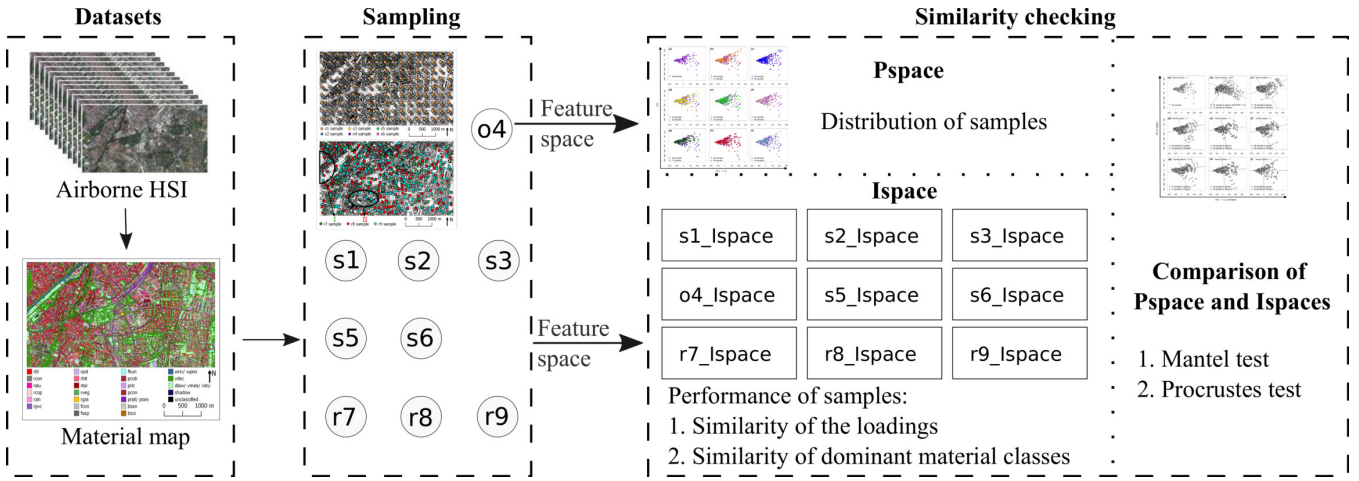
Fig. 2. Schematic of the proposed process for sampling robustness of gradient analysis, including (left dashed) data sets, (middle dashed) sampling, and (right dashed) similarity check. $o4$, $s1$, $s2$, $s3$, $s5$, $s6$, $r7$, $r8$, and $r9$ represent 9 sampling schemes.

any regular permutations or center-to-center distance between samples. Therefore, these sampling schemes are believed to more realistically represent the actual situation of the ground truth distribution in many urban environments.

Fig. 3 shows the distributions of all sampling schemes, in which the surface material map is displayed as a gray scale map of 27 surface material classes listed according to Table I. Both samples of systematic sampling schemes and simple random sampling schemes have a diameter of 100 m. A total of 153 sampling polygons per sampling scheme are generated.

The systematic sampling schemes are evenly distributed over the entire test area, with a center-to-center distance of 300 m between samples (Fig. 3a). The systematic sampling scheme used in Jilge et al. [10] is named as $o4$ and marked by purple color. Six systematically chosen sampling schemes are referred to as $s1$, $s2$, $s3$, $o4$, $s5$, and $s6$, respectively. The six sampling schemes are equidistantly spaced by 25 m in both N-S and W-E directions, i.e., about 35.36 m in NW-SE direction (Fig. 4), which is close to the spatial resolution (30 m x 30 m) of most spaceborne HSIs (e.g., EnMAP).

Samples of three simple random sampling schemes are randomly distributed in the test area (Fig. 3b). Similarly, these three randomly chosen sampling schemes are named $r7$, $r8$, and $r9$, respectively.

B. Derivation of material gradients with PCA

The extraction of material gradients is basically a dimensionality reduction of a sample-by-material matrix, and thus, can be performed by many methods [27]–[29]. Although the resulting material gradients show generally similar characteristics, the available methods differ in their principles, performance, and the fine details of the extracted material gradients. In Jilge et al. [10], material gradients were defined by DCA from the ground sample in the city of Munich, Germany. DCA is often used for gradient analysis in ecology, where studies have analyzed and mapped gradual transitions in the composition of plant species [20], [30], [31]. It assumes that materials have a unimodal distribution along the extracted

(a) Six systematic sampling schemes ($s1$, $s2$, $s3$, $o4$, $s5$, and $s6$)

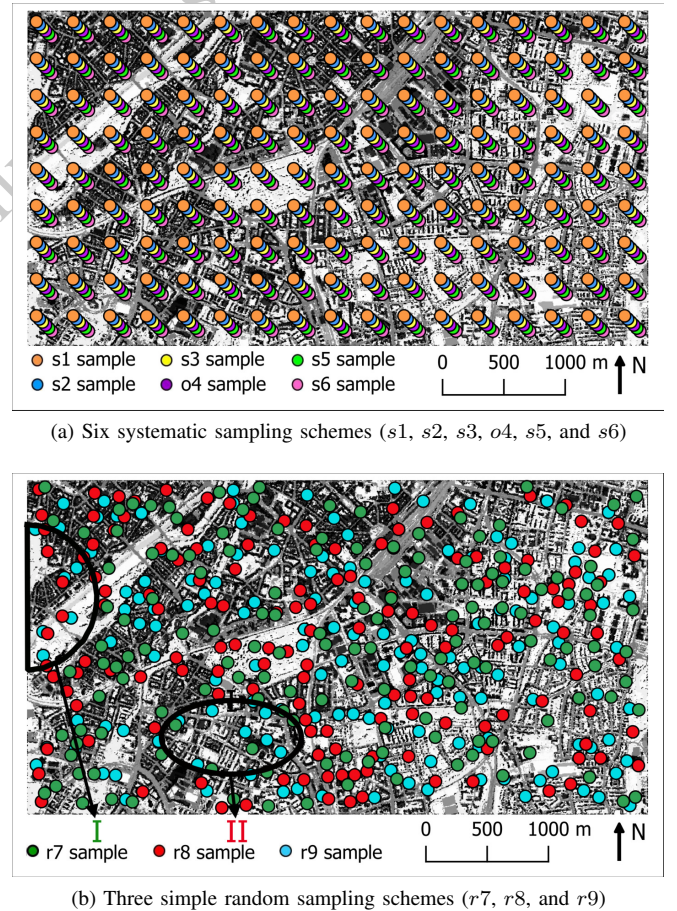(b) Three simple random sampling schemes ($r7$, $r8$, and $r9$)

Fig. 3. Distributions of systematic and simple random sampling schemes. Each sampling scheme is displayed in one color, and circles represent the size and position of samples. Area I is not covered by the $r7$ sampling scheme, and Area II is not covered by the $r8$ sampling scheme. The enlarged systematic sampling schemes are shown in Fig. 4.
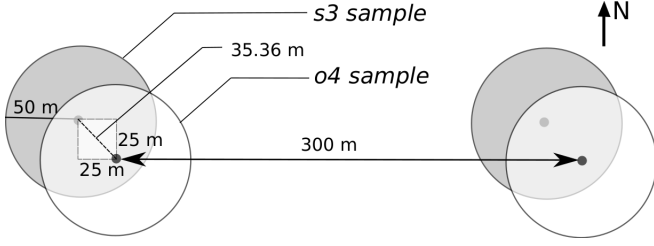
Fig. 4. Enlarged systematic sampling schemes. White circles represent samples from $o4$ sampling scheme, and gray circles show samples from $s3$ sampling scheme. The spacing between adjacent schemes and adjacent samples is shown as a dashed line and a double arrow line between circle centers.

gradients and is therefore well suited for gradients with a pronounced turnover in material composition [32]. With DCA, however, it is difficult to compare resulting gradients with any other gradient feature space, because new observations can not simply be projected into an existing gradient space [10], [33]. In addition, the study [10] has shown that the Munich area does not feature a full material turnover and thus, the unimodal distribution model is not required to describe the material gradients in this area.

In this study we chose PCA to extract material gradients, as it is based on a linear distribution model and allows for a better comparability of different material gradients [34]. PCA is a widely used dimensionality reduction technique [35]–[37], which reduces the dimensionality of data and at the same time retains most of the variations presented in the data set [34], [38]. It achieves the reduction by transforming the data into a new set of variables called principal components (PCs). The PCs are linear combinations of the original variables and are referred to as gradients in terms of their physical significance. The gradients are uncorrelated and hierarchically ordered, so that the first few gradients retain most of the variation presented in all original variables [39]. The number of meaningful gradients is determined according to the broken-stick model, which is considered a stable approach to determining the number of PCs [40], [41].

Subsequently, samples can be projected on the PCs according to their material compositions and the PC loadings to visually assess the similarities and differences among samples. Based on this analysis we may determine whether the samples can be grouped [42]. As the input data here are fractional numbers of material classes, they are fully comparable and for PCA no scaling or centering is needed.

C. Projection of all samples into the Pspace

To get a first impression of the similarity of all sampling schemes, the samples from each sampling scheme were projected into the Pspace. This projection was made with the loadings generated from $o4$ samples [42]. The $o4$ samples were selected to generate the Pspace to be consistent with the sampling scheme used by [10], and because they are ordinary and systematically chosen samples. At first, the Pspace is generated by $o4$ samples with PCA, and includes the first and the second gradients (PCs) according to the broken-stick model. The $o4$ loadings are then extracted by the

transformation from the original material composition matrix into the gradient score matrix. Finally, all samples from other sampling schemes are converted into the Pspace by applying the $o4$ loadings.

D. Sample distribution in the Ispaces

The specific Ispace is the regular gradient space created with PCA by the samples for each individual sampling scheme. Similar to the Pspace, the first and the second material gradients are considered to define each Ispace.

The equation of the PCA is given as follows:

$$A_p \times B_p = C_p \tag{1}$$

where A_p is the material matrix of pth sampling scheme; B_p is the loadings generated by pth sampling scheme; and C_p is the gradient scores of samples in pth sampling scheme. The /redequation (1) expands as follows:

$$
\begin{bmatrix} a_{1,1} & \cdots & a_{1,27} \\ \vdots & \ddots & \vdots \\ a_{153,1} & \cdots & a_{153,27} \end{bmatrix} \times \begin{bmatrix} b_{1,1} & \cdots & b_{1,27} \\ \vdots & \ddots & \vdots \\ b_{27,1} & \cdots & b_{27,27} \end{bmatrix} = \begin{bmatrix} c_{1,1} & \cdots & c_{1,27} \\ \vdots & \ddots & \vdots \\ c_{153,1} & \cdots & c_{153,27} \end{bmatrix} \tag{2}
$$

where $a_{i,j}$ represents the ith sample containing $a_{i,j}$ pixels of material class j; $b_{m,n}$ is the element in loadings; and $c_{i,n}$ represents the gradient score of the ith sample in the nth gradient.

This study only takes the first two gradients $C[i,1]$ and $C[1,2]$ in formula (1) into account, hence only $B[m,1]$ and $B[m,2]$ are considered here.

Two analyses (Pearson correlation and multiple linear regression) are applied to depict the consistency of material gradients and materials among the Ispaces. Pearson correlation analysis is performed by comparing correlated loadings for each sampling scheme, and evaluated using Pearson correlation coefficient. Multiple linear regression analysis is performed in two steps. First, multiple linear regression is applied between material gradient and all material compositions to acquire the weight of each material. Second, the relevance between the material gradient and highly weighted materials (weight > 0.1) is evaluated by adjusted R^2 from further multiple linear regression.

E. Comparison of Pspace and Ispace

Pspace and Ispaces are compared with a Mantel test and a Procrustes analysis [43]–[45]. Both techniques can be used to compare the mutual sample arrangement in the gradient feature space and check whether two neighboring samples in the Pspace are likewise located adjacently in the Ispace. The Mantel test gives an overall estimate of whether the sample distributions in the Pspace and the Ispace match. The Procrustes analysis provides a more detailed assessment and identifies local distortions by quantifying a residual for each data point. In particular, the Mantel test is based on a Pearson correlation between dissimilarity matrices of samples in the Pspace and Ispaces. The dissimilarity matrix of the samples is derived from the Euclidean distances [43]. The significance of the correlations is evaluated by means of permuting rows and columns of the first dissimilarity matrix while a total of 999 permutations are used [46].

IV. RESULTS

A. Sampling

Table I lists the coverage of surface materials per specified sampling scheme. As shown in Table I, each sampling scheme covers all occurring material classes. The cover fractions of common material classes (e.g., $rtil$, $rcon$, $fcon$, $pcob$, $rtar$, $fasp$, $vdec$, $vmea$, and $vdry$) are uniform, mainly varying between 7% and 11%. Nevertheless, cover fractions of several material classes vary substantially among sampling schemes. For instance, $r9$ samples contain only 4% while $r8$ samples contain 22% of synthetic turf in the study area.

B. Distribution of projected Samples in the Pspace

In a first step, all samples from the nine sampling schemes were projected into the Pspace. Fig. 5a shows the distribution of $o4$ samples according to their scores on the first and second material gradients. Along the first material gradient axis, most samples are located at the negative end whereas the number of samples decreases towards the positive direction. The sample distribution ranges between -150 and 250 for the first material gradient, where these values correspond to relative values of the gradient scores. On the second material gradient axis, samples are concentrated around zero, and disperse towards the positive end (about 200) and negative end (about -300). Combining the observations for both material gradients, the samples form a triangular field, with most samples concentrated at the lower left corner, i.e. at the coordinate (-150, 0) and the number of samples gradually decreases towards the other two corners.

Based on the distribution of $o4$ samples, the samples of all other sampling schemes were projected into the Pspace as shown in Fig. 5. The diagrams (Fig. 5b-i) show that all samples are distributed within almost similar triangle field in the Pspace in terms of range and density.

C. Correlation of the Ispaces

The Pearson correlation coefficient [35] was calculated to compare the loadings of all sampling schemes. The coefficients are listed in Table II. In general, the sampling schemes are characterized by high correlations between their loadings. For the loadings on the first material gradient, the Pearson correlation coefficients range between 0.87 ($s1$ and $o4$, $s1$ and $r9$, and $s2$ and $r9$) to 1 ($s1$ and $s2$) and for the loadings on the second material gradient between 0.72 ($s1$ and $o4$, and $s1$ and $r8$) to 0.99 ($o4$ and $r9$), respectively.

The regression parameters represent the multivariate weights of the corresponding materials in the derived material gradients in the Ispaces. The higher the absolute regression parameter, the closer the relationship between the material gradient and the corresponding material. The threshold of highly weighted materials is set as 0.1 since it returns the highest adjusted R^2. For instance, $vdec$, $fasp$, $vmea$, $rtil$, and $fcon$ are highly relevant with the first material gradient in the $s1$ Ispace (Table III). As expected, all Ispaces are similar in terms of the most relevant material classes to the first material gradient. It can be concluded that the first material gradient from different

Ispaces are dominated by these five material classes, though they are produced from different samples. In addition, the second material gradient in $s1$ and also other Ispaces mainly represents $vmea$, $fasp$, $vdec$, $vdry$, and $rtil$, which were the most frequent material class in Table III.

To verify these findings, the regression model was rebuilt between the material gradients and their driving material classes. The resultant adjusted $R^2 = 0.92$ confirms the high relevance between the first material gradient and dominant classes ($vdec$, $fasp$, $vmea$, $rtil$, and $fcon$). Similarly, the second material gradient was regressed with the corresponding five classes ($vmea$, $fasp$, $vdec$, $vdry$, and $rtil$) and an adjusted $R^2 = 0.98$ was returned.

D. Comparison of the Pspace and Ispaces

The Procrustes test, the comparison of sample distributions in the Pspace and Ispaces, is shown in Fig. 6. Since the Pspace is the Ispace of the $o4$ samples, the distribution of $o4$ samples is congruent in both gradient spaces with a Mantel r statistic of 1. Whereas the sample distributions of $s5$, $r8$, and $r9$ sampling schemes only show slight differences, the sample distributions of $s1$ and $s2$ exhibit evident variations (Fig. 6) in the transformation from Ispace to Pspace. In general, all transformations from each Ispace to Pspace can be traced back, and all transformations are not significant. Whereas the sample distributions of $s5$, $r8$, and $r9$ show only minor differences in the transformation from Ispace to Pspace, the sample distributions of $s1$ and $s2$ show a more pronounced dissimilarities (Fig. 6). Overall, the samples show a similar distribution in the Ispaces and Pspace, and the transformations do not lead to major distortions. In another perspective, the Mantel r statistic of 0.97 between $s1$ Ispace and the Pspace, 0.99 between $r7$ Ispace and the Pspace, and 1 between other Ispaces and the Pspace indicate that there are relatively strong correlations between Ispaces and the Pspace. The p-values of 0.001 acquired by all Mantel test indicate that our results are statistically significant at an alpha of 0.05, representing the high credibility of the results.

V. DISCUSSION

The present study aims to investigate whether material gradients are robust among different sampling schemes. In this section, the hypothesis is determined step by step through answering the three research questions.

A. Are material gradients affected by the slight movement of systematically chosen sampling locations?

The similar distributions of samples from six systematic sampling schemes (Fig. 5) provide the impression that the material gradients are robust among slight movement of sample locations in our urban test site.

The high Pearson correlation coefficients (Table II), ranging from 0.87 to 1 between loadings of six systematic sampling schemes for the first material gradient, and from 0.72 to 0.99 for the second material gradient, intuitively demonstrate that the material-to-sample relations from these systematic
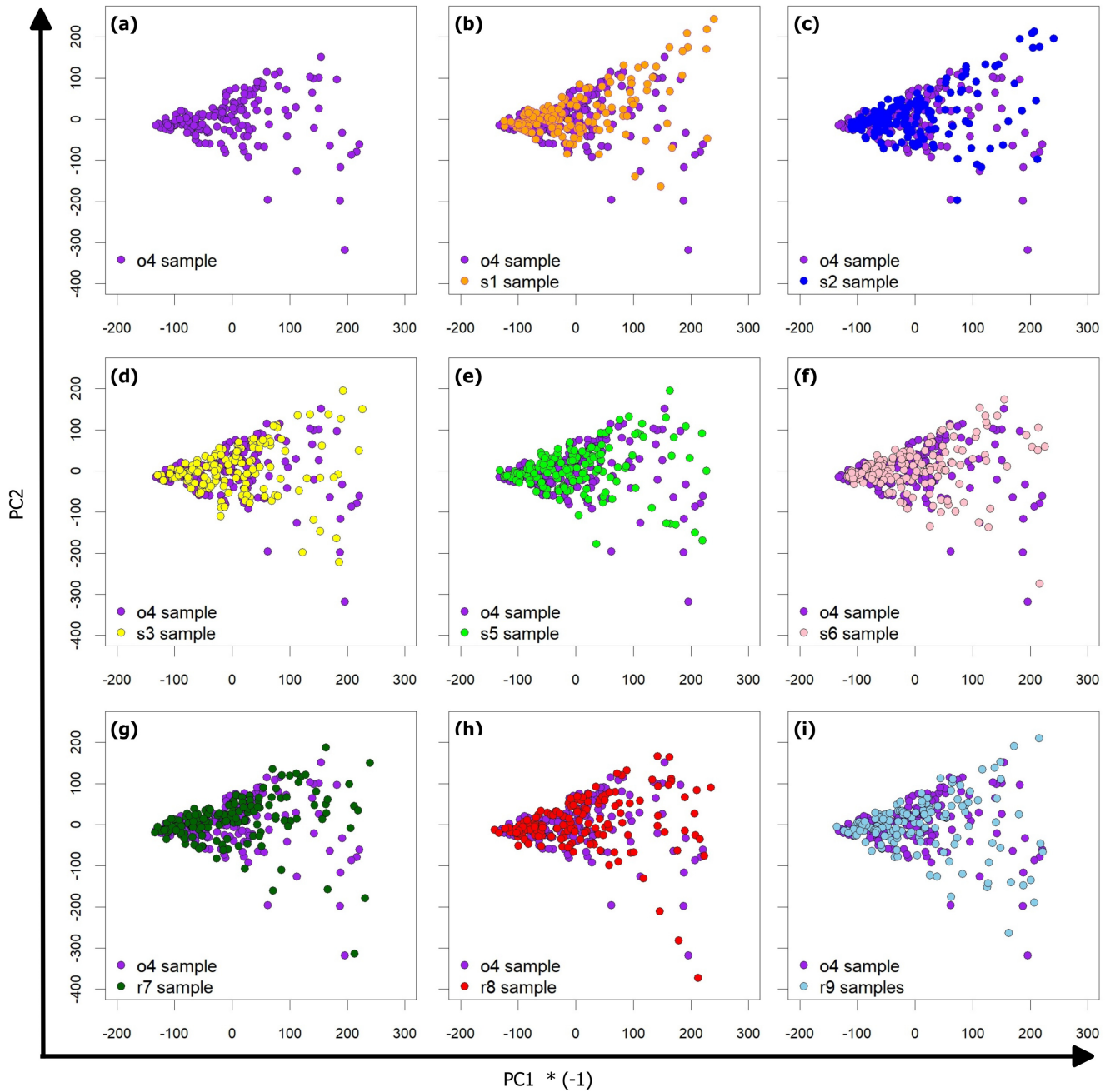
Fig. 5. Similar distribution of samples from six sampling schemes in the Pspace. The X axis represents the first material gradient (PC1) in the inverted direction (*(-1)), and the Y axis represents the second material gradient (PC2). The material gradient axes (PC1 and PC2) have no requirements on the direction. PC1 was inverted for a more intuitive interpretation as in [10], where the negative side presents the artificial materials and the positive side shows more vegetated samples. Each sampling scheme is shown in a specific color which corresponds to the distribution of samples in the surface material map (Fig. 1).

TABLE I
MATERIAL TABLE AND ABBREVIATIONS OF 27 MATERIAL CLASSES, THE MATERIAL COVERAGE OF THE ENTIRE SURFACE MATERIAL MAP (FIG. 1), AND THE MATERIAL COVERAGE IN SAMPLES OF EACH SAMPLING SCHEME.

Abbreviation	Surface material	Total material coverage in material map [pixel]	Material coverage in one sampling scheme/ Material coverage in surface material map [%]								
			$s1$	$s2$	$s3$	$o4$	$s5$	$s6$	$r7$	$r8$	$r9$
$rtil$	roofing tiles	66886	8	8	8	9	9	9	8	8	8
$rcon$	roofing concrete	27440	9	9	8	7	7	8	8	7	10
$ralu$	roofing aluminum	10466	10	9	8	8	9	10	8	8	9
$rcop$	roofing copper	13366	7	7	7	8	8	9	8	9	8
$rzin$	roofing zinc	7607	8	9	8	8	7	5	9	9	8
$rpvc$	roofing PVC	13434	7	8	7	8	8	7	8	9	8
$rpol$	roofing polyethylene	8625	10	12	11	9	8	9	7	10	7
$rbit$	roofing bitumen	14883	10	10	10	8	6	7	9	9	7
$rtar$	roofing tar	29249	8	8	8	8	8	8	9	8	8
$rveg$	vegetated roof	18879	8	9	8	8	8	8	9	8	7
$rgra$	roofing gravel	8206	10	9	9	11	13	13	7	7	8
$fcon$	concrete	42104	8	8	9	10	10	8	8	8	8
$fasp$	asphalt	84854	9	8	8	8	8	8	10	8	8
$fkun$	synthetic turf	3209	10	5	6	9	11	15	5	22	4
$pcob$	cobblestone	47358	9	9	8	8	9	8	8	7	7
$prlc$	loose chippings	20546	7	8	10	10	9	9	7	7	7
$pcon$	concrete slabs	11015	9	9	8	8	8	9	8	7	7
$prail$	railway tracks	10811	8	9	8	7	7	7	9	10	5
$praiv$	vegetated railway tracks	11546	10	10	8	8	7	7	7	9	7
$bsan$	siliceous sand	11765	8	8	8	9	9	9	8	9	11
$bsoi$	humus soil	2978	4	5	5	6	10	11	5	8	14
$wriv$	river	4518	10	10	11	10	7	5	8	9	5
$wpon$	pond	4691	7	8	9	8	9	8	9	9	8
$vdec$	deciduous trees	172784	9	8	8	8	8	8	9	8	8
$vlaw$	lawn	16983	7	8	9	8	8	7	8	7	9
$vmea$	meadow	87525	7	8	8	9	8	8	8	9	9
$vdry$	dry vegetation	35690	9	8	9	9	8	8	8	8	10
total		787418									

sampling schemes are similar. Since the loadings enable to project samples from the material composition matrix to the gradient score matrix in the Ispace, the result demonstrates that all Ispaces formed by material gradients generated from the six systematic sampling schemes are consistent. Regarding the multiple linear regressions between the material gradients and urban surface materials (Table III), it is important to point out that the listed materials only indicate the high-weighted materials on the material gradients, which are considered as dominant materials in this study. $vdec$ dominates the first material gradient at the first place, while $vmea$ dominates the second material gradient for all systematic sampling schemes at the first place. The second and the third dominant materials of the first material gradient are $fasp$ and $vmea$ for all sampling schemes except $o4$. Although the second material gradients represent $vdec$, $fasp$, $vdry$, and $rtil$ in different weights, the aforementioned results still show that the material

gradients generated from different sampling schemes similarly represent 5 materials out of 27 material classes in total.

The results of the Procrustes analysis in Fig. 6a-f show that the arrangement of samples in the Pspace is very similar to the distribution of samples in the Ispaces for all six systematic sampling schemes. The results of the Procrustes test show that the Pspace and Ispaces can be matched by rotating the axes. Consequently, the comparison of the Pspace to the Ispaces demonstrates the robustness of material gradients among the systematic sampling schemes.

One reason for the observed gradient robustness is that the material gradients are dominated by the material classes which cover high fractions in the samples, and the changes of materials covering low fractions are ignored. The dominant material classes ($vdec$, $vmea$, $fasp$, $rtil$, $fcon$, and $vdry$) cover both large parts of the study area (Table I) and are distributed evenly. For example, although cobblestone ($pcob$) covers a

TABLE II
PEARSON CORRELATION COEFFICIENT OF LOADINGS FOR THE FIRST AND THE SECOND MATERIAL GRADIENTS.

	First gradient										Second gradient								
	$s1$	$s2$	$s3$	$o4$	$s5$	$s6$	$r7$	$r8$	$r9$		$s1$	$s2$	$s3$	$o4$	$s5$	$s6$	$r7$	$r8$	$r9$
$s1$		1	0.97	0.87	0.93	0.97	0.95	0.92	0.87	$s1$		-0.87	-0.81	-0.72	-0.77	-0.8	-0.81	-0.72	-0.73
$s2$			0.98	0.88	0.93	0.97	0.94	0.92	0.87	$s2$			0.97	0.85	0.91	0.95	0.93	0.9	0.86
$s3$				0.96	0.98	0.99	0.98	0.98	0.95	$s3$				0.95	0.97	0.98	0.98	0.98	0.95
$o4$					0.99	0.96	0.95	0.99	0.99	$o4$					0.97	0.94	0.97	0.98	0.99
$s5$						0.99	0.98	0.99	0.98	$s5$						0.98	0.97	0.98	0.97
$s6$							0.99	0.98	0.96	$s6$							0.98	0.97	0.95
$r7$								0.98	0.96	$r7$								0.98	0.96
$r8$									0.99	$r8$									0.98
$r9$										$r9$									

TABLE III
MULTIPLE LINEAR REGRESSIONS BETWEEN THE TWO MATERIAL GRADIENTS AND HIGHLY WEIGHTED URBAN SURFACE MATERIALS FOR NINE SAMPLING SCHEMES.

First gradient:

	$s1$		$s2$		$s3$		$o4$		$s5$		$s6$		$r7$		$r8$		$r9$	
	$vdec$	-0.93	$vdec$	-0.93	$vdec$	-0.84	$vdec$	-0.68	$vdec$	-0.77	$vdec$	-0.83	$vdec$	-0.79	$vdec$	-0.76	$vdec$	-0.69
	$fasp$	0.23	$fasp$	0.19	$vmea$	-0.35	$vmea$	-0.57	$vmea$	-0.44	$vmea$	-0.34	$fasp$	0.4	$vmea$	-0.49	$vmea$	-0.58
	$vmea$	-0.15	$vmea$	-0.17	$fasp$	0.23	$rtil$	0.26	$fasp$	0.28	$fasp$	0.3	$vmea$	-0.37	$fasp$	0.27	$fasp$	0.31
	$rtil$	0.13	$fcon$	0.15	$rtil$	0.19	$fasp$	0.26	$rtil$	0.26	$rtil$	0.22	$rtil$	0.18	$rtil$	0.21	$rtil$	0.2
	$fcon$	0.12	$rtil$	0.14	$fcon$	0.18	$fcon$	0.19	$fcon$	0.19	$fcon$	0.15	$fcon$	0.11	$fcon$	0.14	$fcon$	0.13
			$rtar$	0.1	$rtar$	0.1	$rtar$	0.11	$pcob$	0.11	$rtar$	0.1			$rtar$	0.1	$rtar$	0.1
									$rtar$	0.1								

Second gradient:

	$s1$		$s2$		$s3$		$o4$		$s5$		$s6$		$r7$		$r8$		$r9$	
	$vmea$	0.68	$vmea$	-0.88	$vmea$	-0.86	$vmea$	-0.75	$vmea$	-0.78	$vmea$	-0.83	$vmea$	-0.85	$vmea$	-0.81	$vmea$	-0.72
	$fasp$	-0.62	$vdec$	0.26	$vdec$	0.44	$vdec$	0.64	$vdec$	0.54	$vdec$	0.45	$vdec$	0.48	$vdec$	0.56	$vdec$	0.66
	$vdec$	-0.26	$fasp$	0.24	$rtil$	0.13			$rtil$	0.23	$rtil$	0.23	$fasp$	0.13	$rtil$	0.13	$vdry$	-0.14
	$vdry$	0.24	$vdry$	-0.19	$vdry$	-0.12			$vdry$	-0.14	$vdry$	-0.15						
			$rtil$	0.15	$fasp$	0.11			$fcon$	-0.12	$fasp$	0.12						
			$wriv$	-0.14														

larger area than concrete ($fcon$) in the study area, concrete dominates the material gradients compared to cobblestone as concrete is distributed more uniformly than cobblestone. Therefore, the slight movement of systematic sampling has no obvious influence on the material gradients.

B. Are material gradients affected by using random sampling schemes rather than systematic sampling schemes?

The presence of non-stationarity and anisotropy in the spatial data could have a severe impact on the efficiency of systematic sampling [47]. Therefore, the simple random sampling scheme was considered to increase the uncertainty of the material cover fraction in the samples, and thus obtain a broader test scope for the robustness of gradient concept.

As discussed in subsection A, all samples including simple randomly chosen samples are similarly distributed in the Pspace. The samples with low values on the negative side of the second material gradient shown in $o4$, $r7$, and $r8$ by visual interpretation are dominated by deciduous trees ($vdec$). Samples with high values on the positive side of the second material gradient shown in $s1$ are dominated by meadow ($vmea$).

The results for first material gradient in Table II show that the Pearson correlation of loadings between $s1$ and $o4$, $s1$ and $r9$, and $s2$ and $r9$ are lower than others. The results of the second material gradient in Table II show loadings between $s1$ and other sampling schemes, between $s2$ and $o4$, between $s2$ and $r9$ have Pearson correlation values lower than 0.9. Thus, the findings give no systematic differences between the loadings of systematic and simple random sampling schemes.

Also, as mentioned above, the multiple linear regressions between the two material gradients and urban surface materials are similar for both the systematic sampling schemes and the random sampling schemes. The Mantel statistical r is high for each sampling scheme, for example 0.97 for $s1$, 0.99 for $r7$ and 1 for other sampling schemes. The Procrustes test reveals no differences between systematical sampling schemes and random sampling schemes. It implies that the material gradients are not severely affected by sampling strategies. This can be explained by the variance of each material within the sampling schemes that have been used to generate the material gradients (Table I). The material gradient is thereby as mentioned in subsection A largely determined by materials that cover large parts of the study area and at the same time are distributed homogeneously across the study area. For example, Table I shows varying cover fractions of synthetic turf ($fkun$) between the sampling schemes from 4% ($r9$) to 11% ($s5$) to 22% ($r8$). However, since $fkun$ covers just a few urban areas (only 3209 pixels), it has negligible influence on the material gradient.

Another reason for the robustness of the material gradients is linked to the fact that the samples seem to represent the entire study area. Thus, small local differences in the sampling locations do not influence the integral generation and the
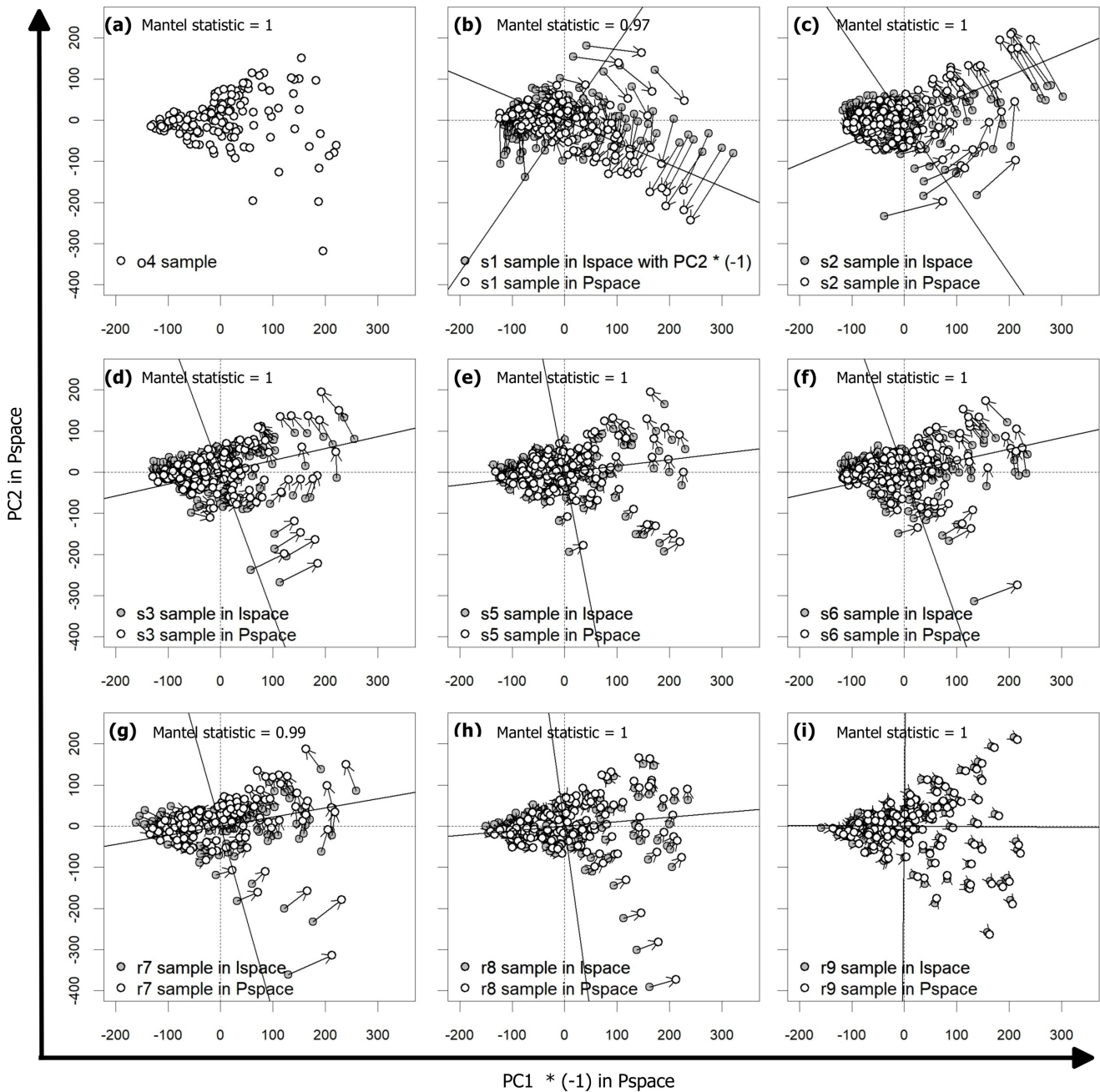
Fig. 6. The comparison of the Pspace and Ispaces in Mantel test and Procrustes test. Each sub-figure shows the path of each sample from Ispaces to Pspace (the Procrustes result) and the statistical result (r) of the Mantel test. The Procrustes test finds the configuration change of each sample in each sampling scheme from Ispace to Pspace. Dashed axes represent the gradient axes of Pspace, and solid axes represent the gradient axes of each Ispace. For $s1$ Ispace, the second material gradient is inverted to show the shortest rotation of $s1$ samples from Ispace to Pspace.

physical significance of the material gradients. For example, as shown in Fig. 3, Area I is not covered by $r7$ sampling and Area II is not covered by $r8$ samples. However, their statistical results shown in Table III show no significant difference.

These observations indicate that Tobler's first law of geography 'everything is related to everything else, but near things are more related than distant things' [48] also applies to the urban material distribution. This distribution shows consequently a positive spatial autocorrelation that characterizes the clustered distribution of the materials. As long as the sampling

schemes represent this clustered distribution sufficiently, the exact location of the samples has no severe influence. Obviously, the spatial scale of this autocorrelation matters. Further testing is needed to analyze these scale dependency of spatial autocorrelation in material distributions across urban areas.

C. What other possible factors could influence the material gradients?

There are several factors influencing the material gradients that need to be discussed. First, we used PCA to define ma-

terial gradients because it allows for an easy comparability of material gradients derived by different sampling schemes (see section III). In comparison to non-metric multidimensional scaling (NMDS) [27], isometric feature mapping (IsoMap) [29], and other unsupervised data reduction methods, PCA provides loadings, which can be used to easily and repeatably transform samples from a material composition matrix to a gradient score matrix. Thus, all samples were projected into one gradient feature space (Pspace) for assessing the robustness of gradients determined by different sampling schemes. One drawback of PCA is that it assumes the class-conditional distributions are Gaussian. The distribution in the real observational data are often not Gaussian but strongly multimodal in some cases [37]. Therefore, PCA might not obtain the best suited material gradients existing in a study area and should only be used for the robustness analysis of material gradients. The PCA-gradient-feature-space generated in this study is not comparable to the DCA-space derived by [10] in scale and number. However, using the same samples, the first material gradient obtained from PCA in this study and DCA in [10] contain similar information on vegetation and artificial material compositions. The second material gradient is different for PCA and DCA. While PCA gradient represents the variety of broad vegetation classes, the gradient obtained by DCA was considered to distinguish urban structures containing different artificial materials.

Second, to map urban material compositions using material gradients, detailed and complete ground truth data are needed that represent the complete variety of material occurrence in the study area. If there is a material not covered by the samples, it cannot be detected or considered in the gradient analysis. If the ground truth data inevitably contains areal errors (also referred to as label noise), the classification accuracy is affected [49]. As the material gradient takes a large amount of input data into account, we consider that a significant amount of label noise is acceptable. Nevertheless, the question of how label noise affects the derived material gradient needs to be investigated in future analyses.

Third, the robustness of material gradient may be weaker in specific urban areas due to a more complex or heterogeneous distribution of urban surface materials. If all samples are distributed in a small part of the investigation area, it is difficult to determine the material gradient to represent the whole variety of surface materials in the investigation area. In other words, the samples should sufficiently cover the whole variety of surface materials in the study area [50]. Thus, this study suggests that the samples should be evenly distributed over the entire study area.

VI. Conclusion

In order to obtain the potential strength of material gradient applied in fuzzy pattern description of urban material compositions using spaceborne HSIs, this paper analyzes the robustness of material gradients in an urban area among different sampling schemes, based on the loadings provided by PCA. The results of this study demonstrate that neither a slight movement of systematic sampling schemes nor simple random sampling schemes largely affect the extracted material gradients. The gradient concept has been proven to be robust for different sampling schemes with the same amount and same size of samples. However, samples shall be well distributed across the study area and need to represent the complete variety of material occurrence in the study area. Future studies should investigate the influence of the size of samples as well as the distance between samples that can also influence the representation of urban surface materials in the gradient space [10]. We suggest to use PCA, if different feature spaces need to be compared to test the transferability of the gradient concept. However, if the objective is to best explore the material composition of a specific urban area, other feature reduction methods seems to be more suitable such as DCA or NMDS.

From the methodical point of view, this study proposes a holistic approach to compare the data transferability of dimensionality reduction methods. The shown experiments and measures can be used not only for testing the transferability of the gradient concept, but might also be useful for other data-driven pattern description approaches.

This study provides a first step towards the transferability of the gradient approach to other urban areas despite their data-driven character. This is very important for the further exploration of spaceborne HSI covering urban areas to characterize urban spaces quantitatively without the need for discrete classification and pure material training information.

References

[1] M. Alberti, "The effects of urban patterns on ecosystem function," *International Regional Science Review*, vol. 28, no. 2, pp. 168–192, Apr. 2005.

[2] T. Oke, *Boundary Layer Climates*. Routledge, London, New York, 1987.

[3] F. Chen, R. Bornstein, S. Grimmond, J. Li, X. Liang, A. Martilli, S. Miao, J. Voogt, and Y. Wang, "Research priorities in observing and modeling urban weather and climate," *Bull. Am. Meteorol. Soc.*, vol. 93, pp. 1725–1728, 2012.

[4] S. van der Linden, A. Okujeni, F. Canters, J. Degerickx, U. Heiden, P. Hostert, F. Priem, B. Somers, and F. Thiel, "Imaging spectroscopy of urban environments," *Surveys in Geophysics*, vol. 40, no. 3, pp. 471–488, May 2019.

[5] L. Guanter, H. Kaufmann, K. Segl, S. Foerster, C. Rogass, S. Chabrillat, T. Kuester, A. Hollstein, G. Rossner, C. Chlebek, C. Straif, S. Fischer, S. Schrader, T. Storch, U. Heiden, A. Mueller, M. Bachmann, H. Mühle, R. Müller, M. Habermeyer, A. Ohndorf, J. Hill, H. Buddenbaum, P. Hostert, S. Van der Linden, P. J. Leitão, A. Rabe, R. Doerffer, H. Krasemann, H. Xi, W. Mauser, T. Hank, M. Locherer, M. Rast, K. Staenz, and B. Sang, "The EnMAP spaceborne imaging spectroscopy mission for earth observation," *Remote Sensing*, vol. 7, no. 7, pp. 8830–8857, 2015.

[6] E. Lopinto and C. Ananasso, "The Prisma hyperspectral mission," in *the 33rd EARSeL Symposium, Towards Horizon*, Matera, 2013, p. 12.

[7] K. Alonso, M. Bachmann, K. Burch, E. Carmona, D. Cerra, R. de los Reyes, D. Dietrich, U. Heiden, A. Hölderlin, J. Ickes, U. Knodt, D. Krutz, H. Lester, R. Müller, M. Pagnutti, P. Reinartz, R. Richter, R. Ryan, I. Sebastian, and M. Tegler, "Data Products, Quality and Validation of the DLR Earth Sensing Imaging Spectrometer (DESIS)," *Sensors*, vol. 19, no. 20, p. 4471, Jan. 2019.

[8] D. Krutz, R. Müller, U. Knodt, B. Günther, I. Walter, I. Sebastian, T. Säuberlich, R. Reulke, E. Carmona, A. Eckardt, H. Venus, C. Fischer, B. Zender, S. Arloth, M. Lieder, M. Neidhardt, U. Grote, F. Schrandt, S. Gelmi, and A. Wojtkowiak, "The instrument design of the dlr earth sensing imaging spectrometer (desis)," *Sensors*, vol. 19, no. 7, p. 1622, Jan. 2019, number: 7 Publisher: Multidisciplinary Digital Publishing Institute.

[9] T. Matsunaga, A. Iwasaki, S. Tsuchida, K. Iwao, R. Nakamura, H. Yamamoto, S. Kato, K. Obata, O. Kashimura, J. Tanii, K. Mouri, and T. Tachikawa, "HISUI status toward FY2019 launch," Valencia, Jul. 2018, pp. 160–163.

[10] M. Jilge, U. Heiden, C. Neumann, and H. Feilhauer, "Gradients in urban material composition: A new concept to map cities with spaceborne imaging spectroscopy data," *Remote Sensing of Environment*, vol. 223, pp. 179–193, Mar. 2019.

[11] R. Mohanty, S. L. Happy, and A. Routray, "A semisupervised spatial spectral regularized manifold local scaling cut with hgf for dimensionality reduction of hyperspectral images," *IEEE Transactions on Geoscience and Remote Sensing*, vol. 57, no. 6, pp. 3423–3435, 2019.

[12] S. Li, W. Song, L. Fang, Y. Chen, P. Ghamisi, and J. A. Benediktsson, "Deep learning for hyperspectral image classification: an overview," *IEEE Transactions on Geoscience and Remote Sensing*, vol. 57, no. 9, pp. 6690–6709, Sep. 2019.

[13] J. Niemela, "Ecology and urban planning," *Biodivers. Conserv.*, vol. 8, pp. 119–131, 1999.

[14] R. Wittig, H. Sukopp, and B. Klausnitzer, *Die ökologische Gliederung der Stadt*. Gustav Fischer Verlag, 1998.

[15] U. Heiden, K. Segl, S. Roessner, and H. Kaufmann, "Determination of robust spectral features for identification of urban surface materials in hyperspectral remote sensing data," *Remote Sensing of Environment*, vol. 111, no. 4, pp. 537–552, 2007.

[16] U. Heiden, W. Heldens, S. Roessner, K. Segl, T. Esch, and A. Mueller, "Urban structure type characterization using hyperspectral remote sensing and height information," *Landscape and Urban Planning*, vol. 105, no. 4, pp. 361–375, Apr. 2012.

[17] W. Heldens, "Use of airborne hyperspectral data and height information to support urban micro climate characterisation," Ph.D. dissertation, University Wuerzburg, Germany, 2010.

[18] M. Bochow, K. Segl, and H. Kaufmann, "An update system for urban biotope maps based on hyperspectral remote sensing data," vol. 1. Bruges: Proceedings 5th EARSeL Workshop on Imaging Spectroscopy, 2007.

[19] S. Schmidtlein, P. Zimmermann, R. Schüpferling, and C. Weiss, "Mapping the floristic continuum: Ordination space position estimated from imaging spectroscopy," *Journal of Vegetation Science*, vol. 18, no. 1, pp. 131–140, 2007.

[20] H. Feilhauer, U. Faude, and S. Schmidtlein, "Combining Isomap ordination and imaging spectroscopy to map continuous floristic gradients in a heterogeneous landscape," *Remote Sensing of Environment*, vol. 115, no. 10, pp. 2513–2524, Oct. 2011.

[21] H. Feilhauer, C. Dahlke, D. Doktor, A. Lausch, S. Schmidtlein, G. Schulz, and S. Stenzel, "Mapping the local variability of natura 2000 habitats with remote sensing," *Applied vegetation science*, vol. 17, no. 4, pp. 765–779, 2014.

[22] C. Neumann, S. Itzerott, G. Weiss, B. Kleinschmit, and S. Schmidtlein, "Mapping multiple plant species abundance patterns-a multiobjective optimization procedure for combining reflectance spectroscopy and species ordination," *Ecological Informatics*, vol. 36, pp. 61–76, 2016.

[23] T. Cocks, R. Jenssen, A. Stewart, I. Wilson, and T. Shields, "The hymaptm airborne hyperspectral sensor: the system, calibration and performance," in *The Proceedings of the 1st EARSeL workshop on Imaging Spectroscopy*. Zurich: The 1st EARSeL workshop on Imaging Spectroscopy, 1998, pp. 37–42.

[24] R. Richter and D. Schlaepfer, "Atmospheric/topographic correction for airborne imagery." 2011.

[25] R. Mueller, M. Lehner, P. Reinartz, M. Schroeder, and R. Mueller, "Evaluation of spaceborne and airborne line scanner images using a generic ortho image processor," *Proc. of High Resolution Earth Imaging for Geospatial Information, ISPRS Hannover Workshop*, vol. 5, 2005.

[26] M. Habermeyer, U. Marschalk, and A. Roth, "Digital elevation model database W42 - a scalable system for spatial data," *The International Archives of the Photogrammetry, Remote Sensing and Spatial Information Sciences*, vol. 37, no. B1, pp. 1253–1258, Jul. 2008.

[27] J. B. Kruskal, "Nonmetric multidimensional scaling: a numerical method," *Psychometrika*, vol. 29, no. 2, pp. 115–129, Jun. 1964.

[28] A. A. Green, M. Berman, P. Switzer, and M. D. Craig, "A transformation for ordering multispectral data in terms of image quality with implications for noise removal," *IEEE Transactions on Geoscience and Remote Sensing*, vol. 26, no. 1, pp. 65–74, Jan. 1988.

[29] J. B. Tenenbaum, V. de Silva, and J. C. Langford, "A global geometric framework for nonlinear dimensionality reduction," *Science (New York, N.Y.)*, vol. 290, no. 5500, pp. 2319–2323, Dec. 2000.

[30] S. Schmidtlein and J. Sassin, "Mapping of continuous floristic gradients in grasslands using hyperspectral imagery," *Remote Sensing of Environment*, vol. 92, no. 1, pp. 126–138, Jul. 2004.

[31] H. Feilhauer and S. Schmidtlein, "Mapping continuous fields of forest alpha and beta diversity," *Applied Vegetation Science*, vol. 12, no. 4, pp. 429–439, 2009.

[32] M. O. Hill and H. G. Gauch, *Detrended correspondence analysis: an improved ordination technique*, advances in vegetation science ed. Dordrecht: Springer, 1980, vol. 2.

[33] R. G. Knox, "Effects of detrending and rescaling on correspondence analysis: solution stability and accuracy," *Vegetatio*, vol. 83, no. 1, pp. 129–136, Oct. 1989.

[34] H. Hotelling, "Analysis of a complex of statistical variables into principal components," *Journal of Educational Psychology*, vol. 24, no. 6, pp. 417–441, 1933.

[35] K. P. F.R.S, "LIII. On lines and planes of closest fit to systems of points in space," *The London, Edinburgh, and Dublin Philosophical Magazine and Journal of Science*, vol. 2, no. 11, pp. 559–572, Nov. 1901.

[36] Jing Wang and Chein-I Chang, "Independent component analysis-based dimensionality reduction with applications in hyperspectral image analysis," *IEEE Transactions on Geoscience and Remote Sensing*, vol. 44, no. 6, pp. 1586–1600, Jun. 2006.

[37] W. Li, S. Prasad, J. E. Fowler, and L. M. Bruce, "Locality-preserving dimensionality reduction and classification for hyperspectral image analysis," *IEEE Transactions on Geoscience and Remote Sensing*, vol. 50, no. 4, pp. 1185–1198, Apr. 2012.

[38] I. Jolliffe, "Principal component analysis," in *International Encyclopedia of Statistical Science*, M. Lovric, Ed. Berlin: Springer Berlin Heidelberg, 2011, pp. 1094–1096.

[39] A. Plaza, P. Martinez, J. Plaza, and R. Perez, "Dimensionality reduction and classification of hyperspectral image data using sequences of extended morphological transformations," *IEEE Transactions on Geoscience and Remote Sensing*, vol. 43, no. 3, pp. 466–479, Mar. 2005.

[40] S. Frontier, "Decrease of eigenvalues in principal component analysis-comparison with broken stick model," *Journal of Experimental Marine Biology and Ecology*, vol. 25, no. 1, pp. 67–75, Nov. 1976.

[41] D. A. Jackson, "Stopping rules in principal components analysis: a comparison of heuristical and statistical approaches," *Ecology*, vol. 74, no. 8, 1993.

[42] M. Ringnér, "What is principal component analysis?" *Nature Biotechnology*, vol. 26, no. 3, pp. 303–304, Mar. 2008.

[43] P. Legendre and L. F. J. Legendre, *Numerical ecology*. Elsevier, Jul. 2012.

[44] K. Mardia, J. Kent, and J. Bibby, "Multivariate analysis," *Probability and mathematical statistics*, 1979.

[45] P. R. Peres-Neto and D. A. Jackson, "How well do multivariate data sets match? The advantages of a Procrustean superimposition approach over the Mantel test," *Oecologia*, vol. 129, no. 2, pp. 169–178, Oct. 2001.

[46] P. Dixon, "VEGAN, a package of R functions for community ecology," *Journal of Vegetation Science*, vol. 14, no. 6, pp. 927–930, 2003.

[47] R. Dunn and A. R. Harrison, "Two-dimensional systematic sampling of land use," *Journal of the Royal Statistical Society: Series C (Applied Statistics)*, vol. 42, no. 4, pp. 585–601, 1993.

[48] W. R. Tobler, "A computer movie simulating urban growth in the detroit region," *Economic Geography*, vol. 46, no. sup1, pp. 234–240, Jun. 1970.

[49] J. Jiang, J. Ma, Z. Wang, C. Chen, and X. Liu, "Hyperspectral image classification in the presence of noisy labels," *IEEE Transactions on Geoscience and Remote Sensing*, vol. 57, no. 2, pp. 851–865, Feb. 2019.

[50] L. Plourde and R. G. Congalton, "Sampling method and sample placement," *Photogrammetric Engineering & Remote Sensing*, vol. 69, no. 3, pp. 289–297, Mar. 2003.

Chaonan Ji received the B.Sc. degree in space science and technology and the M.Sc. degree in space physics from the Shandong University, China in 2015 and 2018, respectively. She is currently pursuing the Ph.D. degree in urban mapping and Earth observation with the Humboldt University of Berlin, Germany and with the German Remote Sensing Data Center, German Aerospace Center, Oberpfaffenhofen, Germany. Her research interests include airborne and spaceborne hyperspectral images classification, gradient analysis and their applications in Earth observation.

Hannes Feilhauer is full professor for Remote Sensing in Geo- and Ecosystem Research at the University of Leipzig. He received his diploma in geoecology at the University of Bayreuth, Germany, his PhD at RFWU Bonn, Germany, and his habilitation at FAU Erlangen-Nuernberg, Germany and worked as visiting professor for Remote Sensing and Geoinformatics at the Institute of Geographical Sciences at Free University of Berlin, Germany. Hannes is interested in all kinds of gradual transitions on the Earth surface and specializes in the use of hyper- and multispectral remote sensing for vegetation mapping.

Marianne Jilge received the B.Eng. degree in cartography and geomedia technology from the University of Applied Sciences Munich, Munich, Germany, in 2012, and the M.Sc. degree in applied geoinformatics from the Paris Lodron University of Salzburg, Salzburg, Austria, in 2014. In 2019 she received the Ph.D. degree from the Ruhr-Univiersity Bochum, Bochum, Germany. She is currently working as a Post-Doc researcher at the German Aerospace Center (DLR) in Oberpfaffenhofen, Germany. Her main research topics are related to urban material mapping with airborne and spaceborne imaging spectroscopy and the determination and mapping of soil information with optical remote sensing time series.

Uta Heiden received her PhD in urban spectroscopy from Technical University of Berlin and GFZ German Research Centre for Geosciences in 2003. Currently, she is researcher at the Remote Sensing Technology Institute (IMF) of the German Aerospace Center (DLR). Uta is interested in application development using airborne and spaceborne imaging spectroscopy data with a focus on the use of material-based reflectance properties of urban surfaces. Recently, Uta has widened her interests towards a better understanding of the function of soils in degrading ecosystems. Uta is Science Coordinator for the spaceborne imaging spectroscopy mission DESIS onboard the ISS and the chair of the "Geoscience Spaceborne Imaging Spectroscopy" Technical Committee (GSIS-TC) of the IEEE Geoscience & Remote Sensing Society. Further, she is member of the Science Advisory Group of the German spaceborne imaging spectrometer mission EnMAP.

Marion Stellmes is currently a researcher and lecturer in the working group Remote Sensing and Geoinformatics at the Institute of Geographical Sciences, Free University of Berlin. She has a strong background in remote-sensing-based monitoring of land degradation and desertification in the Mediterranean and Southern Africa. Marion is specialized in time series analysis of medium- and coarse-resolution remote sensing time series and is focusing in the field of land cover/use change detection.